30. Shen, S.; Sudol, E. D.; El-Aasser, M. S. J Polym Sci Part A: Polym Chem 1994, 32, 1087–1100.
31. Bamnolker, H.; Margel, S. J Polym Sci Part A: Polym Chem 1996, 34, 1857–1871.
32. Paine, A. J. Macromolecules 1990, 23, 3109–3117.
33. Araujo, P. H. H.; Pinto, J. C. Braz J Chem Eng 2000, 17, 383–394.
34. Yamamoto, T.; Fukushima, T.; Kanda, Y.; Higashitani, K. J Colloid Interface Sci 2005, 292, 392–396.
35. Yamamoto, T.; Nakayama, M.; Kanda, Y.; Higashitani, K. J Colloid Interface Sci 2006, 297, 112–121.
36. Sosnowski, S.; Slomkowski, S.; Lorenc, A.; Kricheldorf, H. R. Colloid Polym Sci 2002, 280, 107–115.
37. Slomkowski, S.; Sosnowski, S.; Gadzinowski, M. Polimery 2002, 47, 485–490.

A Versatile Biodegradable Polymer with a Thermo-Reversible/Irreversible Transition

Fumiaki Tanimoto, Yoshiro Kitamura, Tsutomu Ono,* and Hidekazu Yoshizawa

Department of Material and Energy Science, Graduate School of Environmental Science, Okayama University

LETTER

ABSTRACT: A versatile biodegradable thermoresponsive polymer was developed. The polymer has succinimide and isopropylasparamide segments and exhibits a phase transition with thermoreversibility that can be controlled by changing the polymer composition. With fewer succinimide units, the polymer exhibits the type of thermo-reversible phase transition that is characteristic of poly(*N*-isopropylacrylamide) (PNIPAAm). The polymer with a higher proportion of succinimide units exhibits a thermo-irreversible phase transition, resulting in the formation of nanospheres that are stable below the transition temperature. The stable nanospheres are generated by dehydration and subsequent conformational stabilization through an interaction between imide rings. This thermoirreversible phase transition in water provides a simple, oil-free preparation of biodegradable nanospheres.

KEYWORDS: thermoresponsive polymer • irreversible phase transition • poly(aspartic acid) • biodegradable nanosphere • poly(succinimide)

Stimuli-responsive polymers have many potential applications because their properties change dramatically in response to external stimuli such as temperature, pH, and electric field (1−4). Thermoresponsive polymers whose water solubility changes abruptly in response to temperature have been extensively investigated for use in practical applications such as drug delivery vehicles, bioseparation reagents, and surface modifiers, as well as for academic interest to elucidate mechanisms of heat denaturation of proteins (5−7). Attention has mostly been paid to thermoresponsive polymers with lower critical solution temperatures (LCST) in water (8−11). These polymers are water-soluble below the LCST because of their hydrated extended chain conformation, and lose their water solubility above the LCST because of their nonhydrated collapsed chain conformation (12). Although polymer materials are often required to be biodegradable to be useful in fields such as medicine, biology, and environmental science, conventional thermoresponsive polymers such as poly(*N*-isopropylacrylamide) (PNIPAAm) and its copolymers are not degradable. Here, we report a versatile biodegradable thermoresponsive polymer with regulatable thermoreversibility that can be controlled by changing its composition.

Poly(aspartic acid) synthesized by acid-catalyzed polycondensation of L-aspartic acid followed by alkaline hydrolysis is known to be biodegradable and water-soluble (13, 14). Aminolysis of an intermediate product, poly(succinimide) (PSI), with nucleophilic amino compounds is used to form various poly(asparamide)s with functional groups in side chains (15−19). To synthesize thermoresponsive poly(asparamide), we used isopropylamine, which gave a PNIPAAm-like side chain structure, because the thermoresponsivity of PNIPAAm is ascribed to its N-isopropylamide side chain structure. Poly[α,β-(DL-asparate isopropylamide)-*co*-(succinimide)] (designated IPA-PSI) was obtained (Scheme 1) by aminolysis of PSI with isopropylamine in dimethylformamide: the details of the synthesis are described in the Supporting Information. Because poly(aspartic acid)s with dodecyl groups in the side chains have showed biodegradability (16), poly(aspartate) was expected to be a biodegradable polymer. IPA-PSI was gradually converted into poly(aspartate) with thermoresponsive side chains by alkali hydrolysis; therefore IPA-PSI was also expected to be biodegradable.

The mole fraction of isopropylasparamide units in the polymer (hereafter referred to as the degree of substitution) was varied from 30 to 76 mol %. Complete aminolysis of succinimide with isopropylamine did not occur even at the highest mole ratio of isopropylamine to the succinimide unit of PSI in the feed. This might be due to the steric hindrance of the branched alkyl group of isopropylamine because the aminolysis reaction of PSI with propylamine, a nucleophile with a straight alkyl chain, proceeded almost to completion at the same mole ratio of propylamine to the succinimide unit of PSI. Aminolysis of one hydrophobic succinimide unit with one isopropylamine molecule produces one hydrophobic isopropyl group and two hydrophilic amide bonds, thus increasing the hydrophilicity of the polymer. Consequently, the degree of substitution (DS) has a significant effect on the water solubility of the synthesized IPA-PSI. The effect of DS on water solubility is illustrated in Figure 1a. PSI and IPA-PSI with DS < 30 mol % were consistently insoluble in ultra pure water (ultrafiltered with a Milli-Q water purification system) in the temperature range 0−100 °C, and their cloud points were not determined. IPA-PSI with DS > 37 mol %, on the other hand, dissolved freely in ultra pure water. The thermo-responsivity of water-soluble IPA-PSI was of two

* Corresponding author. Tel: +81-86-251-8908. Fax: +81-86-251-8908. E-mail: tono@cc.okayama-u.ac.jp.

Received for review October 17, 2009 and accepted February 16, 2010

DOI: 10.1021/am900705s

Scheme 1. Synthesis of IPA-PSI

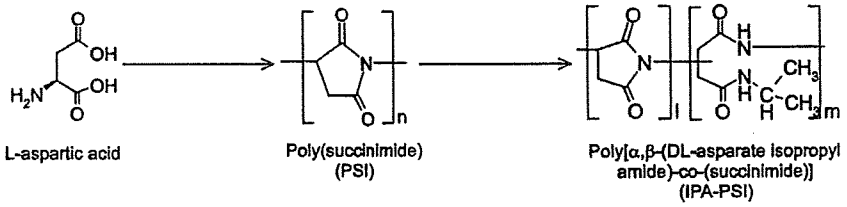

types, corresponding to reversible and irreversible phase transitions, according to the magnitude of DS (Figure 1a).

Aqueous solutions of IPA-PSI with DS > 37 mol % became turbid after being heated to above their cloud point, due to dehydration of the thermoresponsive isopropylamide units. A reversible phase transition was observed for aqueous solutions of IPA-PSIs with DS in the range 62–76 mol %, which were transparent after cooling, as for a conventional thermo-responsive polymer (Figure 1b). By contrast, aqueous solutions of IPA-PSIs with DS in the range 37–56 mol % remained turbid even after cooling (Figure 1b), and the colloid dispersions remained stable for more than one week even after cooling to 0 °C. The temperature dependences of transmittance for 1 wt % aqueous solutions of IPA-PSIs with DS 76 and 37 mol % are shown in Figure 1c together with reference curves for PNPAAm for comparison. The method used to obtain the transmittance curves is given in the Supporting Information. It is apparent from this Figure that the transmittance of the aqueous solution of IPA-PSI with DS = 76 mol % changes more gradually than that of PNIPAAm, and the heating curve does not coincide with the cooling curve (as for PNIPAm). The difference between the heating and cooling curves became increasingly pronounced with decreasing DS, implying that the phase transition of

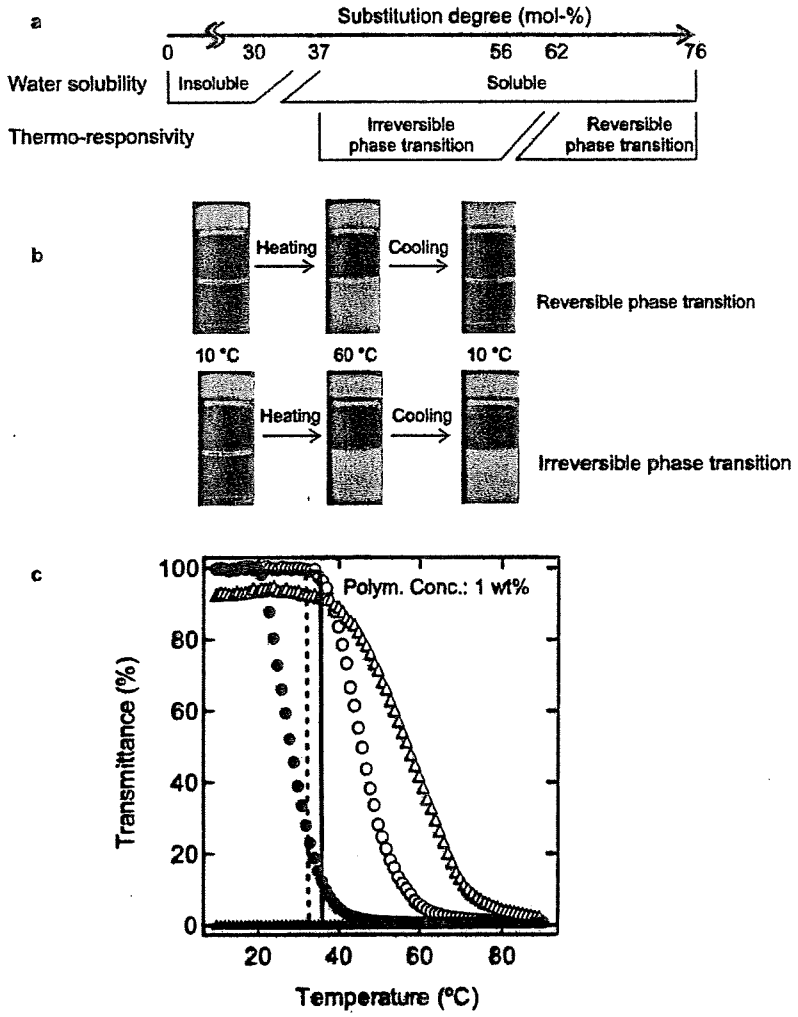

FIGURE 1. Thermoresponsiveness of aqueous solutions of IPA-PSI with various degrees of substitution (DS). (a) Effect of DS on water solubility and thermo-responsivity. (b) Change in appearance of aqueous IPA-PSI with DS = 76 (upper) and DS = 37 mol % (lower). (c) Transmittance of 1 wt % aqueous IPA-PSI solution as a function of temperature. Open triangles, heating curve for IPA-PSI with DS = 37 mol %; filled triangles, cooling curve for IPA-PSI with DS = 37 mol %; open circles, heating curve for IPA-PSI with DS = 76 mol %; filled circles, cooling curve for IPA-PSI with DS = 76 mol %; solid line, heating curve for PNIPAAm; dotted line, cooling curve for PNIPAAm.

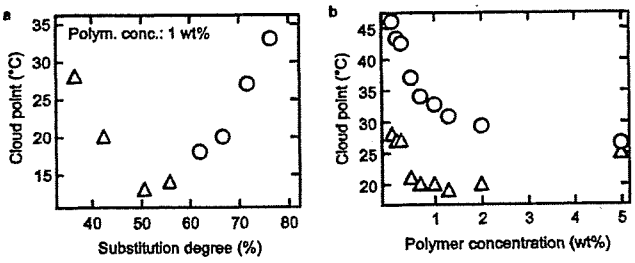

FIGURE 2. Dependence of the cloud point of aqueous IPA-PSI on DS and polymer concentration. (a) Effect of DS on cloud point of 1 wt % aqueous IPA-PSI solution. Triangles, cloud point of IPA-PSI showing irreversible phase transition; circles, cloud point of IPA-PSI showing reversible phase transition. (b) Effect of polymer concentration on cloud point of aqueous IPA-PSI solution. Triangles, DS = 43 mol %; circles, DS = 76 mol %.

IPA-PSI gradually becomes irreversible as DS decreases. The phase transition of IPA-PSI with DS < 60 mol % is irreversible, indicating that the succinimide segments in the main chain significantly affect the reversibility of the phase transition. Moreover, the sharpness of the phase transition decreased as DS decreased. This tendency is attributed to a decrease in the proportion of thermo-responsive isopropylamide units. A similar tendency has been reported for PNIPAAm copolymers with a functional group; the phase transition of PNIPAAm copolymer exhibits a more gradual transition than that of PNIPAAm homopolymer (20, 21).

The effect of DS on the cloud point of 1 wt % aqueous IPA-PSI solution is shown in Figure 2. The cloud point was strongly affected by DS and decreased as DS increased up to 50 mol %. Above that threshold, the cloud point increased as DS increased. It is reasonable to consider this peculiar tendency in two regions of DS. For IPA-PSI with DS > 50 mol %, the variation in the cloud point can be attributed to the hydrophilicity of IPA-PSI. Hydrophilic polymers form strong hydrogen bonds between the amido groups and water molecules, and require more energy to become dehydrated than do hydrophobic polymers, which implies that they have a higher cloud point. This tendency has been reported for copolymers of PNIPAAm and poly(ethylene oxide) (22–24).

For IPA-PSIs with DS < 50 mol %, the variation in the cloud point may be ascribed to increase of the number of intermolecular interaction sites. Furthermore, it seems that reducing the rigidity of the polymer backbone also accelerates intermolecular aggregation. It seems that a five-membered succinimide ring gives more rigidity compared with an aspartate unit because the glass transition temperature of the polymer is increased by decreasing DS of IPA-PSI (see Supporting Information). Consequently, for IPA-PSI with more succinimide rings to collapse, it must overcome a significant energy barrier, resulting in a higher cloud point. In addition, cloud points generally depend on the polymer concentration because aggregation is based on intermolecular interaction: it is known that PNIPAAm shows intramolecular aggregation triggered by dehydration during heating, referred to as a coil–globule transition (25). Figure 2 shows the decrease in the cloud points of IPA-PSI solutions with increasing polymer concentration.

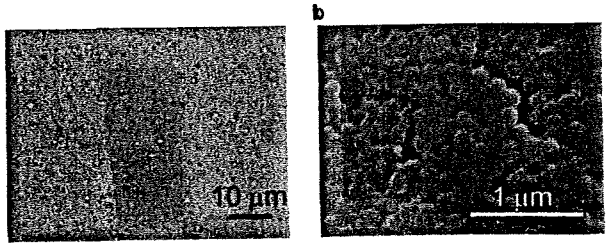

FIGURE 3. Colloid of IPA-PSI with various DS prepared by thermo-induced phase transition. (a) Optical microscopic image of 1 wt % aqueous solution of IPA-PSI with high DS, at 60 °C. (b) SEM image of IPA-PSI particulate prepared by irreversible phase transition of 1 wt % aqueous IPA-PSI solution. The particulate prepared by heating was washed by repeated centrifugation and subsequent dispersion in ultra pure water. The colloid was air-dried before observation.

The colloid induced by the phase transition of IPA-PSI was observed with an optical microscope equipped with a variable-temperature stage. Figure 3a is an image of an aqueous solution of IPA-PSI with high DS at 60 °C (above the cloud point). The figure clearly shows coacervate microdroplets, which formed thermoreversibly. By contrast, the colloid particles from IPA-PSI with low DS cannot be observed by optical microscopy, even though the solution became turbid at temperatures above the cloud point. This implies that very small colloid particles were created. The colloid particles formed by the thermoirreversible phase transition of IPA-PSI with low DS were recovered by centrifugation and resuspended in ultrapure water by agitation, confirming that the phase transition of IPA-PSI with low DS gave a solid product. Figure 3b shows a typical scanning electron microscopy image of the colloid particles prepared from IPA-PSI with low DS. The figure confirms that nanospheres several hundred nanometers in diameter were formed by the irreversible phase transition. Dynamic light scattering analysis of IPA-PSI solution after the irreversible phase transition also indicated the formation of nanospheres, in accordance with the SEM observation.

The strong dependence of cloud point on polymer concentration and the optical microscopic images provide useful information for speculation about the phase transition mechanism of IPA-PSI with high DS. Strong dependence of the cloud point on concentration has been reported for systems that show thermally induced phase separation, such as poly[(*N*,*N*-dimethylacrylamide)-*co*-(*N*-phenylacrylamide)], poly[(*N*-vinylamide)-*co*-(vinyl acetate)], and hydroxylated poly(*N*-isopropylacrylamide) (26–28). These polymers have hydrophilic segments that form hydrogen bonds with water molecules, and show no or only weak endothermic peaks at the cloud point in differential scanning calorimetry (DSC) scans. For the aqueous solution of IPA-PSI with a high DS, an endothermic peak was likewise not detected in the calorimetric study using DSC (see the Supporting Information). The origin of the endothermic peak at the cloud point is the disruption of hydrogen bonding between polymer and water molecules, and the conformational change of the polymer that results in the destruction and reconstruction of a hydrogen-bonded water network. Because of the hydrophilic polyamide backbone chain, the result obtained can be attributed to partial rather than complete dehydration.

LETTER

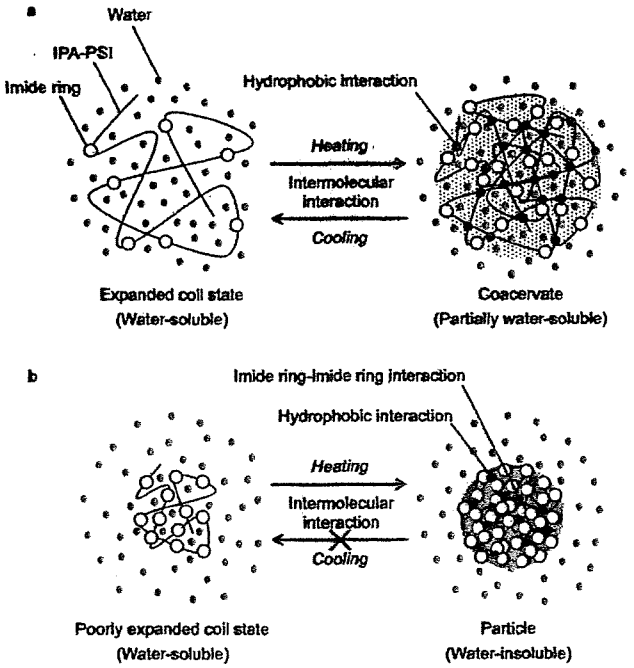

FIGURE 4. Schematic illustration of phase transition of IPA-PSI. (a) phase transition mechanism of IPA-PSI with high DS showing reversible phase transition. (b) Phase transition mechanism of IPA-PSI with low DS showing irreversible phase transition.

These considerations lead to the proposed mechanism of the reversible phase transition of IPA-PSI with high DS shown in Figure 4a. Below the cloud point, IPA-PSI with high DS is in an expanded coil state because of its high hydrophilicity. Above the cloud point, the partially dehydrated IPA-PSI molecules associate each other through hydrophobic interactions. This means that IPA-PSI with high DS involves a lot of dehydrated water molecules through the hydrophilic backbone after the phase transition, forming coacervate droplets.

By contrast, the irreversible phase transition of IPA-PSI with low DS seems to occur by a different mechanism. Because conventional thermo-responsive polymers do not show the irreversible phase transition and do not generate stable nanospheres, IPA-PSI with low DS must possess interaction forces that are sufficiently strong to stabilize particle states even below the transition temperature. The nanospheres were washed with and stored in ultrapure water. Aqueous sodium hydroxide solution was then added dropwise to the colloidal solution with gentle agitation. The turbidity of the colloidal solution gradually disappeared, resulting in a transparent solution. It is known that sodium hydroxide cleaves the succinimide unit without breaking the bond to the IPA-PSI backbone, thus producing polyaspartate. The implication is that the imide rings somehow contribute to stabilizing the particle state of IPA-PSI, and it seems that there is an interaction between the distorted pentagonal rings. This is the basis of the proposed mechanism of the irreversible phase transition, which is shown in Figure 4b. IPA-PSI can dissolve in water at low temperature, but is in a poorly expanded coil state due to its low hydrophilicity. As temperature increases, the molecule is hydrophobized by dehydration, and the hydrophobized molecules are aggregated intermolecularly by hydrophobic interaction. Above the cloud point, IPA-PSI molecules with low DS have few hydrogen-bonding interactions with water molecules and can form solid particles. The interaction between succinimide rings stabilizes the IPA-PSI conformation, resulting in stable particle even below the cloud point.

Generation of a novel biodegradable thermoresponsive polymer whose function can be altered by changing its composition, as described above, enables construction of a general purpose system. IPA-PSI can be chemically modified because the remaining succinimide units can react with nucleophiles. Therefore, IPA-PSI has the potential to replace conventional nondegradable thermo-responsive polymers in fields such as medicine, biology as well as environmental science if the phase transition temperature is tuned around 37 °C. Thus, IPA-PSI may be useful in applications such as drug delivery systems or separation technology. Furthermore IPA-PSI with low DS can be utilized in a novel process for preparing biodegradable nanospheres. This method has several advantages compared with conventional methods of preparation of biodegradable nanospheres. By contrast with most conventional methods, this simple method requires no toxic organic solvent (29, 30). The organic solvent-free process obviates the need for an organic solvent removal process, thus saving energy, reducing organic solvent waste, and eliminating hazards associated with residual organic solvent in drug, food, and environmental applications. The versatile biodegradable thermoresponsive polymer that we report here has the potential for medical, biological, and environmental applications.

Acknowledgment. This study was partly supported by a Grant-in-Aid for Scientific Research (B) (17360383) from the Ministry of Education, Culture, Sports, Science and Technology (MEXT) of Japan.

Supporting Information Available: Experimental procedure to synthesize IPA-PSI derivatives, transmittance curve, and cloud point determination, glass transition temperature, and a DSC result (PDF). This material is available free of charge via the Internet at http://pubs.acs.org.

REFERENCES AND NOTES

(1) Heskins, M.; Guillet, J. E. *J. Macromol. Sci., Chem.* **1968**, *8*, 1441.
(2) Bignotti, F.; Penco, M.; Sartore, L.; Peroni, I.; Mendichi, R.; Casolaro, M.; D' Amore, A. *Polymer* **2000**, *41*, 8247.
(3) Otero, L.; Sereno, L.; Fungo, F.; Liao, Y. L.; Lin, C. Y.; Wong, K. T. *Chem. Mater.* **2006**, *18*, 3495.
(4) Jaycox, G. D. *J. Polym. Sci., Part A: Polym. Chem.* **2004**, *42*, 566.
(5) Chung, J. E.; Yokoyama, M.; Aoyagi, T.; Sakurai, Y.; Okano, T. *J. Controlled Release* **1998**, *53*, 119.
(6) Galaev, I. Y.; Mattiasson, B. *Smart Polymers for Bioseparation and Bioprocessing*; Taylor & Francis: London, 2002.
(7) Okano, T.; Yamada, N.; Sakai, H.; Sakurai, Y. A. *J. Biomed. Mater. Res.* **1993**, *27*, 1243.
(8) Schild, H. G. *Prog. Polym. Sci.* **1992**, *17*, 163.
(9) Akashi, M.; Nakano, S.; Kishida, A. *J. Polym. Sci., Part A: Polym. Chem.* **1996**, *34*, 301.
(10) Zhang, K.; Khan, A. *Macromolecules* **1995**, *28*, 3807.
(11) Thuresson, K.; Karlstrom, G.; Lindman, B. *J. Phys. Chem.* **1995**, *99*, 3823.
(12) Yang, H.; Yan, X.; Cheng, R. *Macromol. Rapid Commun.* **2002**, *23*, 1037.

(13) Vegotsky, A.; Harada, K.; Fox, S. W. *J. Am. Chem. Soc.* **1958**, *80*, 3361.
(14) Roweton, S.; Huang, S. J.; Swift, G. *J. Environ. Polym. Degrad.* **1997**, *5*, 175.
(15) Neri, P.; Antoni, G.; Benvenuti, F.; Cocola, F.; Gazzei, G. *J. Med. Chem.* **1973**, *16*, 893.
(16) Nakato, T.; Tomida, M.; Suwa, M.; Morishima, Y.; Kusuno, A.; Kakuchi, T. *Polym. Bull.* **2000**, *44*, 385.
(17) Takeuchi, Y.; Uyama, H.; Tomoshige, N.; Watanabe, E.; Tachibana, Y.; Kobayashi, S. *J. Polym. Sci., Part A: Polym. Chem.* **2006**, *44*, 671.
(18) Cho, J. Y.; Lee, J.; Gutowska, A.; Tarasevich, B. J.; Sohn, Y. S.; Jeong, B. *J. Drug Delivery Sci. Technol.* **2006**, *15*, 71.
(19) Cho, J. Y.; Sohn, Y. S.; Gutowska, A.; Jeong, B. *Macromol. Rapid Commun.* **2004**, *25*, 964.
(20) Uludag, H.; Norrie, B.; Kousinioris, N.; Gao, T. *Biotechnol. Bioeng.* **2001**, *73*, 510.
(21) Matsukata, M.; Aoki, T.; Sanui, K.; Ogata, N.; Kikuchi, A.; Sakurai, Y.; Okano, T. *Bioconjugate Chem.* **1996**, *7*, 96.
(22) Priest, J. H.; Murray, S. L.; Nelson, R. J.; Hoffman, A. S. *ACS Symp. Ser. 350* **1987**, 255.
(23) Galaev, I. Y.; Mattiasson, B. *Enzyme Microb. Technol.* **1993**, *15*, 354.
(24) Ito, S. *Kobunshi Ronbunshu* **1990**, *47*, 467.
(25) Wang, X.; Qiu, X.; Wu, C. *Macromolecules* **1998**, *31*, 2972.
(26) Miyazaki, H.; Kataoka, K. *Polymer* **1996**, *37*, 681.
(27) Yamamoto, K.; Serizawa, T.; Akashi, M. *Macromol. Chem. Phys.* **2003**, *204*, 1027.
(28) Maeda, T.; Kanda, T.; Yonekura, Y.; Yamamoto, K.; Aoyagi, T. *Biomacromolecules* **2006**, *7*, 545.
(29) Cristallini, C.; Enriquez De Grassi, G.; Guardines, L.; Gaussmann, R. *Appl. Biochem. Biotechnol.* **1984**, *10*, 267.
(30) Giunchedi, P.; Conte, U. *STP Pharma Sci.* **1995**, *5*, 276.

Materials Letters 64 (2010) 969–971

Contents lists available at ScienceDirect

Materials Letters

journal homepage: www.elsevier.com/locate/matlet

PEG–PLA nanoparticles prepared by emulsion solvent diffusion using oil-soluble and water-soluble PEG–PLA

Makoto Muranaka, Ken Hirota, Tsutomu Ono *

Department of Material and Energy Science, Graduate School of Environmental Science, Okayama University, 3-1-1 Tsushima-Naka, Okayama 700-8530, Japan

ARTICLE INFO

Article history:
Received 4 December 2009
Accepted 27 January 2010
Available online 1 February 2010

Keywords:
Nanomaterials
Polymers
Colloidal carrier
Emulsion solvent diffusion

ABSTRACT

Poly(ethylene glycol)-*block*-polylactide (PEG–PLA) nanoparticles were prepared through the oil-in-water (O/W, ethyl acetate/water) emulsion technique using oil-soluble PEG–PLA in the presence of water-soluble PEG–PLA as a surfactant. The particle diameter decreased with increasing water-soluble PEG–PLA concentration, the smallest averaged diameter was 75 nm. From these results, it was found that water-soluble PEG–PLA acted as a surfactant which prevents further coalescence of droplets. In addition, the particles diameter decreased with increasing hydrophile–lipophile balance of oil-soluble PEG–PLA in the absence of water-soluble PEG–PLA. In contrast, the particle diameter was constant in the presence of water-soluble PEG–PLA. Therefore, the capability of water-soluble PEG–PLA as a surfactant was more excellent than that of oil-soluble PEG–PLA.

1. Introduction

The colloidal carriers which are injectable drugs are classified into nanoparticles [1], micelles [2] and liposomes [3]. They are a good promising way to keep the drug activity and control its release to specific tissues. In particular, biodegradable nanoparticles, poly(ethylene glycol)-block-polylactide (PEG–PLA) nanoparticles with PEG corona has been interested as drug carriers [4–10]. A PEG layer protects the drug-loaded PLA core from their interaction with plasma proteins and phagocytic cells so that it prolongs the blood circulation times. Furthermore, the biodegradability of PLA takes an advantage in controlling drug release.

To date, PEG–PLA nanoparticles are prepared by a phase separation method [4–6], emulsion solvent evaporation [7–10]. The phase separation method has a disadvantage such as low encapsulation efficiency due to the lack of driving force for drug incorporation during the preparation of nanoparticles. On the other hand, PEG–PLA nanoparticles obtained by emulsion solvent evaporation have higher encapsulation efficiency by keeping drugs in the emulsion droplets stabilized with surfactants [11,12]. However, PEG–PLA nanoparticles with less than 180 nm in diameter have not been obtained by the technique. To accumulate drugs around cancer tumor, enhanced permeability and retention (EPR) effect is expectable if the drug carrier is less than 150 nm [13]. Therefore, it is worth developing the preparation technique of smaller PEG–PLA nanoparticles in a range of 50–100 nm for a wide range of chemotherapy.

Since surfactant is a crucial factor in the stability of emulsion and in the control of droplet diameter affecting the size of resultant nanoparticles, the selection of surfactant is most important for the emulsion solvent evaporation; besides, the available surfactant for medical use is limited in terms of toxicity and biocompatibility. Hence we considered the surfactant used in this method from the following viewpoints; (1) simply synthesized (designable), (2) no toxic, (3) biocompatible and (4) water-soluble one. Accordingly, we concluded PEG–PLA, which is the same diblock copolymer as the particle matrix except the water solubility. PEG–PLA are easily synthesized by ring-opening polymerization of lactide using poly(ethylene glycol) monomethyl ether (MeOPEG) as an initiator in the presence of stannous 2-ethylhexanoate as a catalyst [14]. In addition, the chain length of PEG and PLA is controllable by altering the molecular weight of MeOPEG used and the feed concentration of MeOPEG in the polymerization of lactide, respectively. Furthermore, organic solvent also plays a key role for this study. Although chloroform or dichloromethylene solves both PEG and PLA segments, ethyl acetate is a good solvent for only PLA segment. That is why it is possible that PEG–PLA acts as a surfactant in an ethyl acetate–water system.

In this article, we developed PEG–PLA nanoparticles less than 100 nm in diameter by emulsion solvent diffusion method using oil-soluble and water-soluble PEG–PLA. This simple process facilitates highly drug-loaded nanocarrier for cancer therapy without any residual hazardous agent.

2. Experimental

2.1. PEG–PLA synthesis

PEG–PLA was synthesized by ring-opening polymerization of D, L-lactide (Purac, Netherland) using MeOPEG (Mw=4000, NOF, Japan) as an initiator in the presence of tin(II) 2-ethylhexanoate (Wako Pure Chemical Industries, Ltd., Japan) as a catalyst. D, L-lactide, MeOPEG and a

* Corresponding author. Tel./fax: +81 86 251 8908.
E-mail address: tono@cc.okayama-u.ac.jp (T. Ono).

0167-577X/$ – see front matter © 2010 Elsevier B.V. All rights reserved.
doi:10.1016/j.matlet.2010.01.076

toluene solution of tin(II) 2-ethylhexanoate were placed into an ampoule, which was sealed under reduced pressure and immersed in an oil bath at 403 K. The polymerization was conducted for 24 h. After cooling, the reaction mixture was dissolved in chloroform and excess hexane was added. After the precipitated polymer was recovered and was washed with 2-propanol, subsequent drying under reduced pressure at 313 K was conducted.

2.2. PEG–PLA nanoparticle preparation

PEG–PLA nanoparticles were prepared by the emulsion solvent diffusion method. 2 ml of the polymer solution (60 mg of oil-soluble PEG–PLA in ethyl acetate) was emulsified by sonication (15 s; 160 W) into a 4-ml aqueous solution dissolved water-soluble PEG–PLA (0.01–5 wt.% w/v). The resultant emulsion was diluted in 100-ml aqueous solution. Finally, the nanoparticles were isolated by centrifugation at 15,000 rpm for 60 min and washed three times with water and were freeze dried.

2.3. Characterization

The weight-averaged molecular weight (*Mw*) and the polydispersity index (*Mw/Mn*) of the synthesized polymer were measured using a gel permeation chromatography (HLC 8120, Tosoh, GPC) on the basis of the polystyrene standards with tetrahydrofuran as an eluent. The morphology of PEG–PLA nanoparticles was characterized by scanning electron microscope (S-4700, Hitachi, SEM). The diameter of PEG–PLA nanoparticles in water was characterized by dynamic light scattering measurement (Zetasizer, Malvern, DLS) at 293 K.

3. Results and discussion

3.1. PEG–PLA synthesis

PEG–PLA was successfully obtained by ring-opening polymerization of D, L-lactide using MeOPEG as an initiator. The analytical results of synthesized copolymer are summarized in Table 1. To investigate the effect of the hydrophile–lipophile balance (HLB) of PEG–PLA on the diameter of PEG–PLA nanoparticles, six kinds of PEG–PLA with different HLB were synthesized.

3.2. PEG–PLA nanoparticles preparation

Fig. 1 shows the SEM image of PEG_4–PLA_{29} nanoparticles obtained by the emulsion solvent diffusion method using PEG_4–PLA_1 as a surfactant. The averaged diameter of nanoparticles was 75 nm and the diameter distribution was narrow. In addition, although the averaged-droplet diameter in the emulsion was 360 nm, the diameter became smaller when the emulsion was diluted with a great amount of aqueous solution. From these results, the nanoparticles were formed by the diffusion of ethyl acetate from the droplets to aqueous bulk solution. It was caused by high water solubility of ethyl acetate (8.7%, w/v). Furthermore, the ratio of the peak at 3.9 ppm (OCH_2CH_2 for PEG) to the one at 5.2 ppm (CH for PLA) in the ^1H NMR spectrum of PEG_4–PLA_{29} nanoparticles was almost the same as that of PEG_4–PLA_{29}.

Table 1
Molecular structures of PEG–PLA.

Code	PEG–PLA *Mw*	PLA *Mw*	PEG–PLA *Mw/Mn*	HLB	Solubility
PEG_4–PLA_{36}	40,000	35,600	1.61	2.21	Oil-soluble[a]
PEG_4–PLA_{29}	33,000	28,600	1.32	2.68	Oil-soluble[a]
PEG_4–PLA_{10}	14,000	9600	1.34	6.28	Oil-soluble[a]
PEG_4–PLA_7	11,000	6600	1.14	8.23	Oil-soluble[a]
PEG_4–PLA_1	5200	800	1.07	16.6	Water-soluble[b]

[a] Highly soluble in ethyl acetate.
[b] Highly soluble in water.

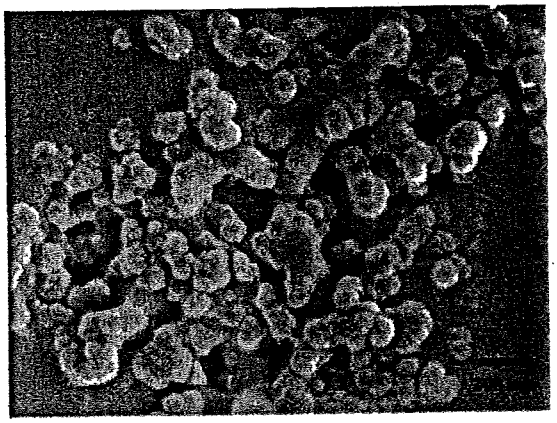

Fig. 1. SEM image of PEG_4–PLA_{29} nanoparticles prepared by the emulsion solvent diffusion method using PEG_4–PLA_1 as a surfactant; [PEG_4–PLA_{29}] = 3.3 wt.%, [PEG_4–PLA_1] = 5.0 wt.%.

It was confirmed by GPC measurement of the nanoparticles that the peak of PEG_4–PLA_1 was nothing. Therefore, this indicates that almost all PEG_4–PLA_1 are removed from the nanoparticles by the aqueous washing.

3.3. Diameter control of PEG–PLA nanoparticles

Fig. 2 shows the effect of PEG_4–PLA_1 concentration on the diameter of PEG–PLA nanoparticles. As shown this figure, the nanoparticles with a size range of 75–360 nm were obtained by altering the PEG_4–PLA_1 concentration. In addition, the particle diameter decreased with increasing the PEG_4–PLA_1 concentration. This result clarify that PEG_4–PLA_1 plays a role of surfactant which prevents further coalescence of droplets and reduces the interfacial tension between ethyl acetate and water. Moreover, the particle diameter of PEG_4–PLA_7 nanoparticles was smaller than that of PEG_4–PLA_{29} nanoparticles at low polymer concentrations. Thus, all synthesized PEG–PLA behave as a surfactant and influence the resultant particle diameter of PEG–PLA nanoparticles. Fig. 3 shows the effect of HLB of oil-soluble PEG–PLA on the diameter of PEG–PLA nanoparticles. The particle diameter decreased with increasing HLB of oil-soluble PEG–PLA in the absence of PEG_4–PLA_1. As considered above, this result proved that all PEG–PLA acted as a surfactant for the preparation of PEG–PLA nanoparticles. When using PEG_4–PLA_{36}, which has a longest PLA chain in this study, it formed stable micelles (core: PEG, shell: PLA) in ethyl acetate. Therefore, the number of PEG_4–PLA_{36} adsorbed on the interface decreased, and then the diameter of nanoparticles increased. In contrast, the particle diameter was constant in the presence of PEG_4–PLA_1. The oil-

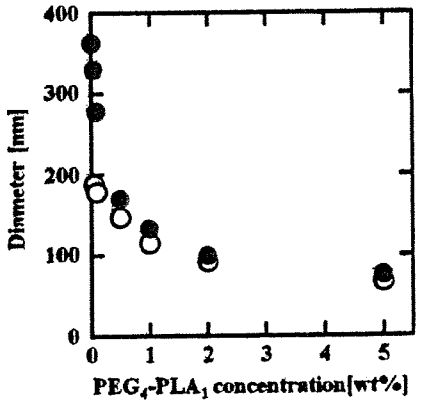

Fig. 2. The effect of PEG_4–PLA_1 concentration on the diameter of PEG–PLA nanoparticles; open key: PEG_4–PLA_7 (3.3 wt.%), closed key: PEG_4–PLA_{29} (3.3 wt.%).

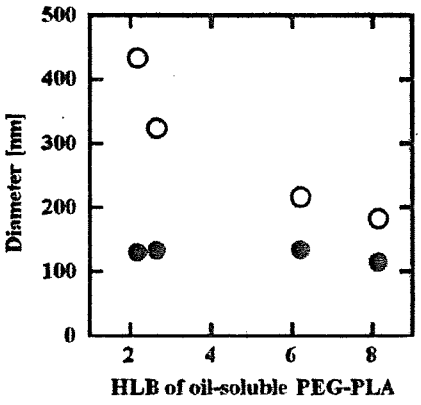

Fig. 3. The effect of HLB of oil-soluble PEG–PLA (5.3 wt.%) on the diameter of PEG–PLA nanoparticles; open key: in the absence of PEG_4–PLA_1, closed key: in the presence of PEG_4–PLA_1 (0.1 wt.%).

soluble PEG–PLA and PEG_4–PLA_1 competitively adsorb onto the oil–water interface. The capability of PEG_4–PLA_1 was more excellent than that of oil-soluble PEG–PLA due to large mobility of PEG_4–PLA_1 which has low molecular weight.

4. Conclusions

In summary, PEG–PLA nanoparticles were prepared with oil-soluble PEG–PLA through oil-in-water emulsion solvent diffusion method in the presence of water-soluble PEG–PLA as a surfactant. The nanoparticles with a size range of 75–360 nm were obtained by altering the water-soluble PEG–PLA concentration. In addition, the particles diameter decreased with increasing HLB of oil-soluble PEG–PLA in the absence of water-soluble PEG–PLA, whereas the particle diameter was constant in the presence of water-soluble PEG–PLA. Therefore, it was found that the oil-soluble PEG–PLA also acted as a surfactant and that water-soluble PEG–PLA showed more excellent capability for a surface-active reagent than oil-soluble one and facilitated the formation of PEG–PLA nanoparticles less than 100 nm in diameter. Consequently, this preparation technique would provide a wide range of applications such as drug delivery system.

References

[1] Gong X, Milic T, Xu C, Batteas JD, Drain CM. J Am Chem Soc 2002;124:14290–1.
[2] Harada A, Kataoka K. J Am Chem Soc 1999;121:9241–2.
[3] Yuasa M, Oyaizu K, Murata H, Sahara Y, Hatsugai T, Ogata A. J Oleo Sci 2007;56:87–93.
[4] Thirumala G, Trevo R, Touraj E, Martin CG, Snjezana S, Lisbeth I, Stanley SD. Int J Pharm 2000;199:95–110.
[5] Riley T, Stolnik S, Heald CR, Xiong CD, Garnett MC, Illum L, Davis SS, Purkiss SC, Barlow RJ, Gellert PR. Langmuir 2001;17:3168–74.
[6] Ren J, Hong HY, Ren TB, Teng XR. Mater Lett 2005;59:2655–8.
[7] Perez C, Sanchez A, Putnam D, Ting D, Langer R, Alonso MJ. J Control Release 2001;75:211–24.
[8] Vila A, Gill H, McCallion O, Alonso MJ. J Control Release 2004;98:231–44.
[9] Sant S, Nadeau V, Hildgen P. J Control Release 2005;107:203–14.
[10] Jo YS, Kim MC, Kim DK, Kim CJ, Jeong YK, Kim KJ, Muhammed M. Nanotechnology 2004;15:1186–94.
[11] Rosa GD, Iommelli R, Rotonda MIL, Miro A, Quaglia F. J Control Release 2000;69:283–95.
[12] Yang YY, Wan JP, Chung TS, Pallathadka PK, Ng S, Heller J. J Control Release 2001;75:115–28.
[13] Maeda H, Wu J, Sawa T, Matsumura Y, Hori K. J Control Release 2000;65:271–84.
[14] Zhu KJ, Xiangzhou L, Shilin Y. J Appl Polym Sci 1990;39:1–9.

ポリ乳酸系ナノ粒子の調製と光線力学的治療への応用

小野　努[*1]・大河原賢一[*2]

Tsutomu Ono・Ken-ichi Ogarawa

[*1] 岡山大学大学院環境学研究科　准教授　博士(工学)　[*2] 医歯薬総合研究科　准教授　博士(薬学)

1．はじめに

光線力学的治療(PDT)は，通常の抗癌剤を用いた化学療法とは異なり，外部から腫瘍近傍にのみ光を照射することで，局所的な抗癌効果を期待する低侵襲性治療のひとつである．日本でも1994年に早期の肺癌，食道癌，胃癌，子宮頸部癌に対して厚生労働省(当時は厚生省)の認可を受け，1996年には保険採用されている．PDTは腫瘍を選択的に壊死させることが可能なことから，安全性に優れ，外科施術を必要としない患者のクオリティーオブライフ(Quality of life，QOL)にも考慮した低侵襲性の抗癌治療法あり，今後の普及が強く期待される治療法である．

しかしながら，今日十分に普及できていない原因として，治療に必要なレーザーが大型で高価だったことや早期癌のみの適応だったことに加え，他に目立った副作用がないなかで唯一といえる副作用が光過敏症であり，それが意外に大きな問題であったことが原因だと考えられている[1]．PDTで用いる薬物は一般にいう光増感剤である．光を感受して励起し，励起三重項状態から酸素へのエネルギー移動によって一重項酸素を生成し，その一重項酸素が細胞を壊死させていくというものである．そのため，静脈投与によって患部以外の細胞へ取り込まれた光感受性物質が自然光によっても作用することで光過敏症が生じるため，PDTを受けた患者は治療後に一定期間の暗室での生活を余儀なくされる．これまでに厚生労働省で認可されている光感受性物質には，Photofrin®，talaporfin sodium(Laserphyrin®)，加齢黄斑変性症(患者数約35万人)を対象としたVerteporfin(Visudyne®)の3種類があり，第一世代のPhotofrin®は投与後に約4週間の遮光が必要であったが，第二世代のLaserphyrin®は3～7日間に短縮されているものの依然遮光期間が不可欠である．このように，患者のQOLを向上させるためには更なる副作用軽減が必要であり，PDT用薬物キャリアによるドラッグデリバリーの改善には大きな期待が込められている．

本研究では，そのような研究背景をもとにして，高分子ナノ粒子を薬物キャリアとしたPDTへの応用を研究目的としている(図1)．疎水性の高い光増感剤を高分子ナノ粒子に内封し，薬物内封ナノ粒子には高い血中滞留性を付与することで，長時間血液中を循環し，腫瘍近傍における未成熟血管壁から内部へ浸透して滞留するEPR効果(enhanced permeation and retention effect)[2]を利用した薬物の集積を目指している．ここで，血中滞留時の薬物徐放が大きいと正常細胞への光増感剤の分布が広がり，上述のような光過敏症を誘発すると考えられるため，本研究のDDSに関するコンセプトは薬物を安定にナノ粒子中へ保ちつつ高い血中滞留性を確保し，高価なターゲティング素子を付与することなく，PDTの特性を活かした局所的低侵襲治療を実現することにある．医学系や薬学系研究者とは異なるケミカルエンジニアらしいアプローチによって材料調製プロセスを新たに構築し，PDTの臨床応用を目指したこれまでの研究成果を紹介する．

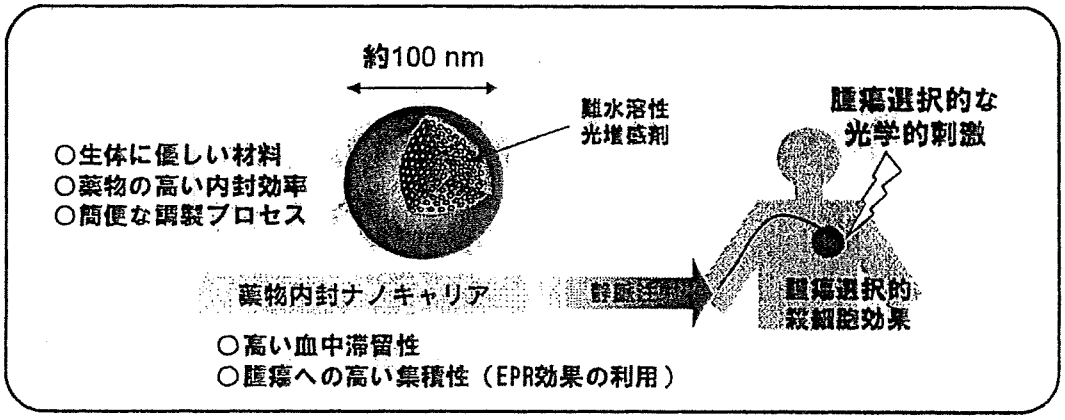

図１　薬物キャリアを利用した光線力学的治療（Photodynamic Therapy，PDT）の概念図

２．高分子治療

高分子治療とは，Polymer therapeutics という言葉を日本語に置き換えたものであるが，全ての場合で高分子そのものが病気を治すわけではないことから内容を的確に表現しているとは言い難い．ただ，少なからず高分子が治療効果を大きく改善することに貢献してきたことは紛れもない事実であろう．Polymer therapeutics は，1980 年代に Ringsdorf や Duncan によって提唱された言葉であり[2~4]，より広義な意味を持つ造語である“nano-medicine”として使われることもある．高分子にはさまざまなユニットを組み込むことができることから，生体内において効果的に薬物を機能させる高分子とのコンジュゲートがデザイン可能である（図２）．高分子を積極的に薬物とリンクさせ，化学的治療効果の改善に利用されてからはまだ 30 年余りであるが，その間薬物の高分子化，高分子ー薬物コンジュゲート，高分子ータンパク質コンジュゲート，高分子ー核酸コンジュゲートなど，さまざまな形態で高分子が利用され，溶解性の制御や生体内での安定性の向上などを実現し，最近の報告では十数種類の製品が既に市場へ流通し，同程度の数が臨床試験中にある[5]．

一方，高分子と薬物を共有結合的にリンクさせなくても，薬物を内封した高分子材料を調製できれば，ドラッグデリバリー担体として利用できる．この際，高分子材料開発における高分子の分子構造デザインは，薬物の内封挙動と密接に関係しており，高分子会合体および高分子微粒子の内部にいかにして薬物を内封するかを目的として微粒子調製プロセスを検討していくことが，最終的な高分子製剤の有効性の鍵を握ると考えられる．なかでも“高分子ミセル”は，東京大学の片岡らの研究グループによって開発された国産の技術であり，そのうち NK105 はパクリタキセルを内封する DDS 製剤として国内にて第 II 相試験が行われている最中である[6]．高分子ミセルは，ブロック共重合体の Self-assembly によって得られる 50 nm 以下の会合体であり，高分子ミセル構造形成のドライビングフォースである疎水性相互作用を利用して，ミセル内部に難水溶性の薬物を内封するこ

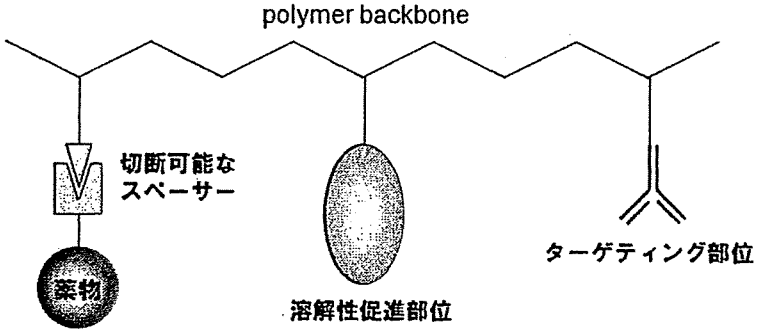

図２　Ringsdorf の提唱する高分子ー薬物コンジュゲートのモデル[2]

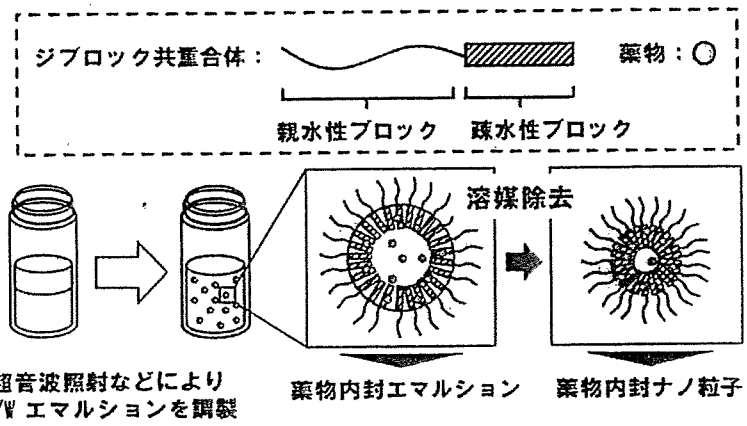

図３　溶媒拡散法によるジブロック共重合体を用いたナノ粒子調製法

とが可能になる．最近では，デンドリマーのコア部分に薬物を内封したナノスケールの薬物キャリア[7]や光増感剤自体をデンドリマー化してアニオン性を付与し，カチオン性を有するジブロック共重合体でポリイオンコンプレックス(PIC)ミセルを形成したPDTへの応用も検討されている[8]．

３．溶媒拡散法によるPEG-PLAナノ粒子

さまざまなポリマー製剤が開発されるなか，われわれは溶媒拡散法によるナノ粒子調製を行っている．本手法は，まずoil-in-water(O/W)エマルションを調製し，ジブロック共重合体の片方のユニットが溶解する有機溶媒を系中から除去することによって溶解性の乏しいユニット部分の析出を促し，結果として固体のコアを持ち，溶媒へ溶解性の高い高分子鎖を表面に持つナノ粒子が調製できる(図３)．

生体内への投与を考慮し，ナノ粒子を構成する成分として，抗原性を示さず生体適合性の高いポリエチレングリコール(PEG)鎖と生分解性高分子であるポリ乳酸(PLA)鎖のジブロック共重合体(PEG-PLA)を用いることとした(図４)．PEGユニットは水に易溶であるが，PLAユニットは水

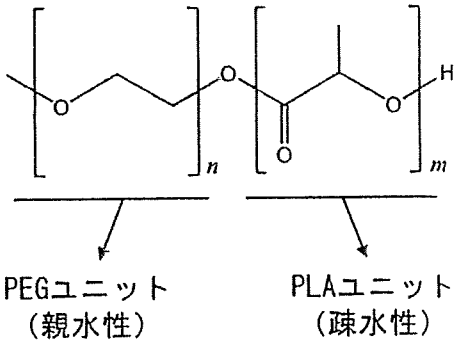

図４　PEG-PLA ジブロック共重合体の分子構造

に不溶であり，そのブロック共重合体PEG-PLAは両ユニットの組成によって親水性か疎水性が決まる．本研究では，表１のようなPLA鎖長の異なる水溶性PEG-PLAと油溶性PEG-PLAの二種類を合成し，ナノ粒子調製を行った．さらに溶媒拡散法では，酢酸エチルを油相として用いることで，PEG-PLAによるエマルションの安定化が期待できる．なぜなら，酢酸エチルに対してはPLAユニットが易溶であるのに対してPEGユニットは不溶であるため，ジブロック共重合体は水-酢酸エチル界面へ配向しやすい状況を生み出している．

なお，本研究で用いているPEGとPLAはいずれも広く用いられている知名度の高い高分子であ

表１　用いたPEG-PLAジブロック共重合体の組成

Sample No.	MeOPEG *Mw*	PEG-PLA *Mw*	PLA *Mw*	PEG-PLA *Mw/Mn*	PLA/PEG	HLB値	溶解性
o-PEG-PLA	5,000	42,000	37,000	1.30	7.81	2.27	油溶性
w-PEG-PLA	5,000	6,000	1,000	1.05	0.29	15.55	水溶性

り，そのブロック共重合体もまた数多くの研究が行われている．当然，生体への安全性に優れていることから，ドラッグデリバリー担体としても数多くの研究が行われている[9~13]．特に，疎水性抗癌物質であるパクリタキセル(Paclitaxel)を内封したPEG-b-PLAミセル(Genexol-PM)は，現在乳癌や肺癌を対象としてPhase Ⅱ試験が行われている[6,14]．ほとんどの場合，PEG-PLAを用いた薬物内封体は高分子ミセルとして調製されており，ブロック共重合体中のPLA/PEG比が比較的1に近いものがよく用いられている．これは，高分子ミセルが水媒体中で調製されるため，ポリマー自体の水溶性と有機溶媒の除去に伴う自己会合体形成に必要な親-疎水性バランスを考慮したものであるといえる．それゆえ，本研究のコンセプトに基づき，薬物キャリアを設計するためには高分子ミセル構造よりも安定に薬物を内封させることを目的としてPLAユニットを増やし，油溶性PEG-PLAを有機溶媒に添加して固化させることで，PEGを表面に持ちPLAをマトリックスとしたPEG-PLAナノ粒子の調製を行ってきた．粒子化した内部に薬物を内封することで，副作用の原因となる血中滞留時の薬物徐放は抑えられ，さらに担体への高効率な薬物内封が可能な調製プロセスの構築が期待される．

一般に高分子ミセルの調製方法としては，有機溶媒の減圧留去(液中乾燥)法，透析，キャスト法などが用いられる．いずれの手法においても薬物を溶解させている有機溶媒を除去することで，薬物を内封した高分子ミセルの形成を行う．この有機溶媒としてよく用いられているジクロロメタンは生体に対しても有害であり，薬剤として調製する際には僅かな残留もない調製法が求められる．本実験で用いている酢酸エチルもまた同様に溶媒拡散法によって除去を行うが，医薬品添加物規格，食品添加物公定書にも認められた比較的安全性の高い有機溶媒である．酢酸エチルはまた，水にも若干溶解することから，大量の水による希釈操作のみで常温で簡単に有機溶媒除去が可能な溶媒拡散法に適した有機溶媒といえる．

まず，酢酸エチル相に所定量の油溶性PEG-PLAを溶解させ，超音波照射を行ってO/Wエマルション液滴を調製したところ，超音波出力の増加とともに得られる液滴が若干小さくなることが分かった(図5)．溶媒拡散法によって最終的に得られたナノ粒子は，調製された液滴径を反映して平均径も減少するが，超音波出力を高くしても220 nm程度が限界であり，EPR効果を期待するには粒径が大きすぎる．従来の研究においても，同様に比較的PLA/PEG比の大きなPEG-PLAを用いた場合は200 nm以上の粒子しか得られておらず[15]，静脈注入する抗癌剤としては更なる調製手法の改良が求められていた．

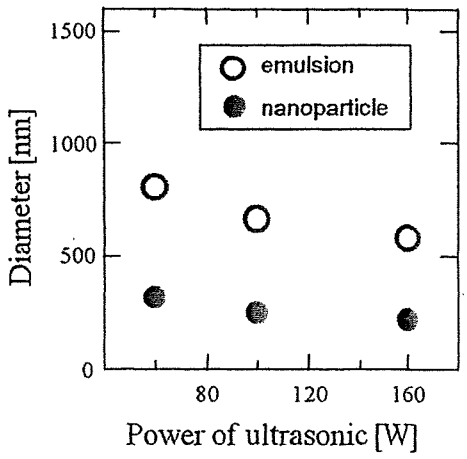

図5　粒径におよぼす超音波出力の影響

そこで，本研究では超音波照射で調製される液滴径を小さくすることを目的として界面活性剤の導入を検討し，製剤調製時に余計な試薬の混入を防ぐために，界面活性剤としての役割を担う水溶性PEG-PLAを合成した．そして，ナノ粒子マトリクス成分として重要な油溶性PEG-PLAとの同時使用を試みた．その結果，水溶性PEG-PLAとの併用によって超音波照射によるエマルション液滴径は大きく低下し，100 nm以下のナノ粒子を得ることに成功した(図6)．図7のように走査型電子顕微鏡(SEM)の写真からも，100 nm以下のナノ粒子が得られていることが示されている．得られたナノ粒子組成を^{1}H-NMRによって測定したところ，ナノ粒子を純水で洗浄することで，水溶性PEG-PLAはほとんどナノ粒子内には残らないことが確認された．また，実際に光増感剤であるフォトプロトポルフィリンIXジメチルエステル[16]を内封した際も，ほぼ同等のナノ粒子調製挙動を示すことを確認している．調製時の光増感剤濃度を増加させると，内封率も大きく低下したが，

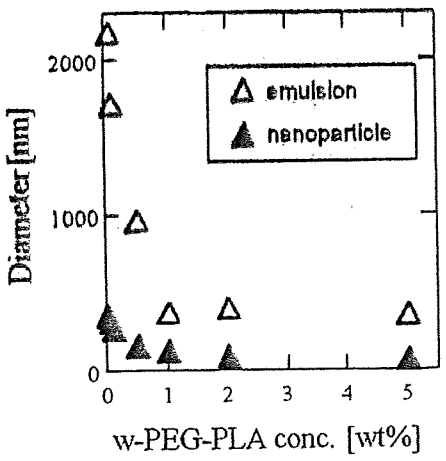

図6　粒径におよぼす水溶性 PEG-PLA(w-PEG-PLA)濃度の影響

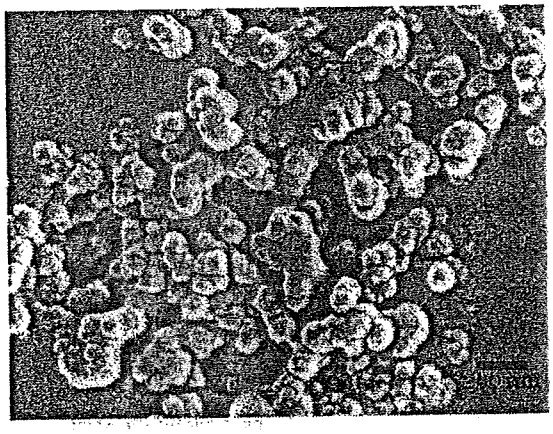

図7　PEG-PLA を用いて調製したナノ粒子の SEM 写真

これは光増感剤の酢酸エチルへの溶解度によるものであり，飽和溶解度以下の濃度であればほぼ100%の薬物内封効率を達成することができる．

このように，溶媒拡散法によって簡便で高効率な薬物内封ナノ粒子調製を実現することができたことから，PDT における薬物キャリアとしての性能を評価するために *in vitro*(生体外)実験および *in vivo*(生体内)実験を行った．

4．光線力学的治療への応用

マウス結腸癌由来細胞(C26 細胞)を播種した細胞培養ディッシュ上に，本ナノ粒子分散水溶液を添加し，一定時間培養後，培地交換して光照射を行った．光照射装置は市販の光源ランプに 500 nm 以下の光を遮断するフィルターを装着したものを用い，赤色光の照射を実施した．このときの細胞生存率を MTT assay により行ったところ，光増感剤の最終濃度が約 50 nM でも光照射によりほぼ全ての細胞が死滅することが分かった．また，細胞のナノ粒子への曝露時間の増加に伴い細胞生存率も低下することから，ナノ粒子から細胞へ光増感剤の物質移動が起こっていることが示唆された．

次に，本ナノ粒子の体内での薬物動態を調査するために，^{3}H 標識ナノ粒子を調製し，C26 細胞をマウス背部皮下に移植して腫瘍体積が約 500 mm^3 に達した時点で ^{3}H 標識ナノ粒子を尾から静脈注射した．その結果，血液中での滞留性の指標となる AUC(% of dose/mL·hr)値を算出すると，2070 と非常に高い値を得た．一般的なリポソーム製剤よりも高い値であり，24 時間後でも 3 割以上の薬物が体内循環していることが分かった．このときの各臓器への移行も定量した結果，5〜10 時間までに一時的に肺や脾臓に集積するもののその後低下したのに対して，図8から分かるように，腫瘍への蓄積は 25 時間後まで着実に増加を続けており，EPR 効果による薬物集積が機能していることが確かめられた．また，図8から筋肉への集積がほとんどないことが示唆されており，これは光過敏症などの副作用抑制を大きく期待させる結果であるといえる．

さらに，C26 細胞担癌モデルマウスを作製して，担癌マウスへの PDT 効果を実証した．腫瘍体積が 100 mm^3 に達した時点で，3 mg/kg となるように光増感剤内封ナノ粒子水溶液を静脈投与した．図9には，その後の腫瘍サイズの増加を示す．その結果，参照実験群と比較しても単回照射群で腫瘍

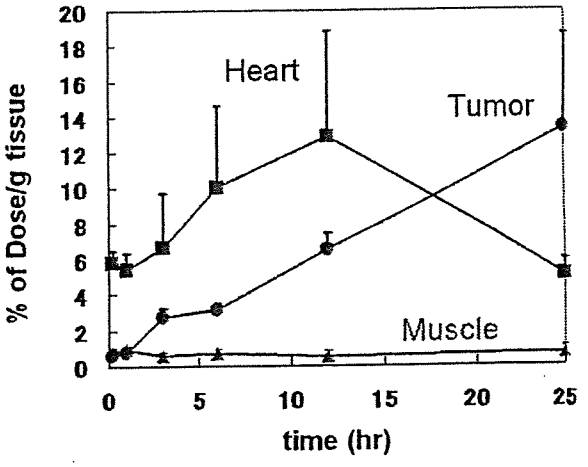

図8　^{3}H 標識ナノ粒子を用いた担癌マウスに対する静脈内投与後の各臓器への移行

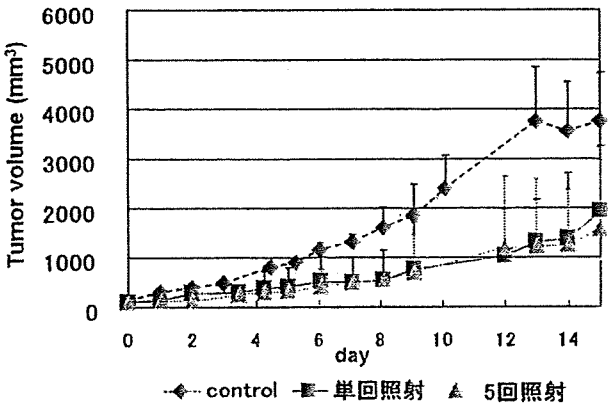

図9　担癌マウスへの PDT 結果(Control：ナノ粒子の代替として PBS 投与，単回照射群：投与 12 時間後に赤色光(l >500 nm)を腫瘍局所に 5 分間照射，5 回照射群：投与 6, 12, 24, 36, 48 時間後に同様の光照射)

抑制効果を有意に示していることがわかる．この間，マウスの体重変化はほとんどなく，PDT による腫瘍の増殖抑制が達成されたことが *in vivo* 実験で示された．図8の結果と合わせて，本研究で目指す高い血中滞留性を保ち薬物徐放を抑えたナノ粒子は，PDT のためのドラッグキャリアとして極めて有効であるといえる．

5．おわりに

溶媒拡散法を用いたナノ粒子調製において，水溶性 PEG-PLA と油溶性 PEG-PLA を合わせて使用することで，エマルション液滴の微小化を達成した結果，EPR 効果の期待できる 100 nm 以下のポリ乳酸系ナノ粒子を調製することに成功した．本手法は，ほぼ 100%に近い内封率で疎水性薬物をナノ粒子内に内封することが可能であり，有害な物質がほとんど残留しない PEG-PLA と薬物のみで構成された生体適合性ナノ粒子を常温，低エネルギーで調製できる簡便な方法である．光増感剤を内封したポリ乳酸系ナノ粒子は，colon26 細胞を用いた *in vitro*(生体外)実験において，極めて薬物濃度が低い条件でも光照射による殺細胞効果を示し，PDT における有効性を示すことができた．さらに，担癌マウスを用いた *in vivo*(生体内)実験においては，血中での高い滞留性を示し，PDT による腫瘍増殖抑制を明らかにすることができた．本ナノ粒子調製法においては，光増感剤以外の疎水性薬物を同時に封入することも可能なため，他の作用機序を有する難水溶性抗癌剤との多剤併用治療にも有効であると期待される．現在は，この有望な薬物ナノキャリアを活用して抗腫瘍効果を向上させることを目指すとともに，本手法を用いた薬剤調製デバイスの開発も検討中である．また，本研究で用いたポルフィリン内封ナノ粒子は，製剤調製時の安全性に関する問題点をほとんど有さず，PDT による治療効果も期待できる基礎的知見を得ていることから，今後は臨床応用に向けた取り組みを進めていきたいと考えている．

最後に，本研究は厚生労働科研費医療機器開発推進研究事業：ナノメディシン研究の助成を得て推進できましたことに感謝申し上げます．また，本研究を遂行するにあたり多大な協力を頂いた株式会社アスコルバイオ研究所顧問 阪田功様(旧㈱光ケミカル研究所常務取締役)，当研究室の廣田健君，渡邉貴一君，自然科学研究科特任助教 村中誠君，医歯薬総合研究科 白石太朗君にこの場を借りて厚く御礼申し上げます．

参考論文

1) 奥仲哲弥，「PDT 適応拡大への課題」，第19回日本光線力学学会学術講演会抄録集，p.18
2) Y. Matsumura, H. Maeda, A New Concept for Macromolecular Therapeutics in Cancer Chemotherapy : Mechanism of Tumoritropic Accumulation of Proteins and the Antitumor Agent Smancs, *Cancer Res.*, 46, 6387-6392 (1986)
3) L. Gros, H. Ringsdorf, H. Schupp, *Angew. Chem. Int. Ed.* 20, 305-325 (1981)
4) R. Duncan, The dawning era of polymer therapeutics, *Nat. Rev. Drug Discov.*, 2, 347 (2003)
5) M.J. Vicent, H. Ringsdorf, R. Duncan, Polymer therapeutics : Clinical applications and challenges for development, *Adv. Drug Delivery Rev.*, 61, 1117-1120 (2009)
6) 加藤　健，パクリタキセル内包ミセル NK105 の臨床試験の状況，*Drug Delivery System*, 24-1, 28-34 (2009)
7) E.R. Gillies, J.M.J. Frechet, Dendrimers and dendritic polymers in drug delivery, *Drug Discovery Today*, 10, 35-43 (2005)
8) N. Nishiyama, Y. Nakagishi, Y. Morimoto, P.-S. Lai, K. Miyazaki, K. Urano, S. Horie, M. Kumagai, S. Fukushima, Y. Cheng, W.-D. Jang, M. Kikuchi, K. Kataoka, Enhanced photodynamic cancer treatment by supramolecular nanocarriers charged with dendrimer phthalocyanine, *J. Controlled Release*, 133, 245-251 (2009)
9) L. Yang, X. Wu, F. Liu, Y. Duan, S. Li, Novel biodegradable polylactide/poly(ethylene glycol) micelles prepared by direct dissolution method for controlled delivery of anticancer drugs, *Pharm. Res.*, 26, 2332-2342 (2009)
10) P. Jie, S.S. Venkatraman, F. Min, B.Y.C. Freddy, G.L. Huat, Micelle-like nanoparticles of star-branched PEO-PLA copolymers

as chemotherapeutic carrier, *J. Controlled Release*, **110**, 20-33 (2005)

11) L. Chen, Z. Xie, J. Hu, X. Chen, X. Jing, Enantiomeric PLA-PEG block copolymers and their stereocomplex micelles used as rifampin delivery, *J. Nanopart. Res.*, **9**, 777-785 (2007)

12) X. Wang, Y. Wang, X. Chen, J. Wang, X. Zhang, Q. Zhang, NGR-modified micelles enhance their interaction with CD13-overexpressing tumor and endothelial cells, *J. Controlled Release*, **139**, 56-62 (2009)

13) L. Liu, C. Li, X. Li, Z. Yuan, Y. An, B. He, Biodegradable polylactide/poly(ethylene glycol)/polylactide triblock copolymer micelles as anticancer drug carriers, *J. Appl. Polym., Sci.*, **80**, 1976 (2001)

14) T.-Y. Kim, D.-W. Kim, J.-Y. Chung, S.G. Shin, S.-C. Kim, D.S. Heo, N.K. Kim, Y.-J. Bang, Phase I and pharmacokinetic study of Genexol-PM, a cremophor-free polymeric micelle-foumulated paclitaxel, in patients with advanced malignancies, *Clinical Cancer Res.*, **10**, 3708 (2004)

15) R. Gref, P. Quellec, A. Sanchez, P. Calvo, E. Dellacherie, M.J. Alonso, Development and characterization of CyA-loaded poly(lactic acid)-poly(ethylene glycol) PEG micro- and nanoparticles. Comparison with conventional PLA particulate carriers, *Eur. J. Pharm. Biopharm.*, **51**, 111-118 (2001)

16) 特願 2008-118187

An emulsion generating microchannel device oscillated by 2.25MHz ultrasonic vibrator

Takuya Harada[1], Takefumi Kanda[1], Koichi Suzumori[1], Tsutomu Ono[2], Sotaro Iwabuchi[2], Kazuyuki Ito[2], Ken-ichi Ogawara[3] and Kazutaka Higaki[3]

[1]Graduate School of Natural Science and Technology, Okayama University, Okayama, JAPAN
[2]Graduate School of Environmental Science, Okayama University, Okayama, JAPAN
[3]Graduate School of Medicine Dentistry and Pharmaceutical Sciences, Okayama University, Okayama, JAPAN

In this study, an emulsion generating device by an ultrasonic vibration and a microchannel has been used to obtain emulsions. The process to generate emulsion consists of Y-type microchannel and ultrasonic device. Once micro meter size emulsions were generated by Y-type microchannel, after that, micro emulsions are sonicated by the ultrasonic vibration and the microchannel to obtain emulsions. Though the diameter of emulsions was 30μm by using Y-type microchannel, sonicated emulsions' diameter was about 200nm. In addition, as the applied voltage increased, sonicated emulsions became smaller and distribution became sharper.

Keywords : emulsion, sonication, ultrasonic vibration, microchannel, emulsification

1. Introduction

An emulsification is an important technique and used in many fields such as cosmetics, food production and medical science. Especially, monodisperse emulsion is very useful because it improves the quality and stabilities of products and facilitates the control of properties 1).

A lot of emulsification techniques have been studied 2). For example, a high pressure homogenization 3, 4), a membrane emulsification 5, 6), a microchannel emulsification 7, 8) and a PIT (Phase Inversion Temperature) method 9, 10).

Some devices used an ultrasonic vibration to generate emulsions 11-15). These devices use a cavitation effect to generate emulsions. The cavitation effect is occurred when a liquid is irradiated by ultrasonic, the pressure amplitude of the applied sound source reaches a certain minimum threshold and some micro bubbles in the water are collapsed 13, 14). The formation of cavitaion is growth and subsequent collapse of microbubbles caused by the pressure fluctuations of the acoustic wave 11). Cavitational collapse generates intense local heating, high pressure and liquid jet stream 13). By these functions, emulsions are generated.

From some references, ultrasonic emulsification has certain trends 11-15).

1. As the irradiation power increases, the dispersed phase droplet size decreases.
2. As the residence time increases, the dispersed phase droplet size decreases
3. As the concentration of the dispersed phase increases, the require irradiation power increases to reduce the dispersed phase droplet size.

In fact, the irradiation power, the residence time and the concentration of the dispersed phase influence the dispersed phase droplet size and the quality (stability) of emulsion.

A simple way to generate emulsions by ultrasonic is by immersion of a transducer horn into the solution and using cavitation. However, as this driving frequency is around 20 kHz, noise is made loudly. Furthermore, as this process is batch process, contamination of the emulsions can't be avoided. In addition, entire devices become large because transducer horn is large.

We have studied generation of emulsions by a torsional Langevin-type transducer and a micropore plate 16). However, it is difficult to generate nano size emulsions because emulsions' diameter is depend on micropore diameter.

The aim of this study is to fabricate an emulsion generating device using an ultrasonic vibration and a microchannel. By integrating the ultrasonic device and the microchannel, the small device and a flow process will be realized. In addition, contamination of the emulsions can be avoided.

2. Structure and material

2.1 Emulsion generating system

The process to generate emulsion consists of Y-type microchannel and ultrasonic device. Schema of the emulsion generating system is shown in **Fig. 1**. Once oil and water are supplied by syringe pumps to Y-type microchannel, micro emulsions are generated because of the fluid shear fore caused by two flow rate difference 9). After that, micro emulsions are sonicated by an ultrasonic vibration and a microchannel to obtain emulsions.

By using this method, the flow process can be conducted and contamination of the emulsions can be avoided. Furthermore, as it is possible to integrate the Y-type

microchannel and ultrasonic device, small emulsification device can be fabricated.

Figure 2 shows the photographs of the Y-type microchannel. The Y-type microchannel is four-layer structure and consists of two stainless steel block, a thin Y-microchannel and a glass substrate. The thin Y-microchannel is sandwiched in between the stainless steel and the glass substrate. The Y-type microchannel is made of stainless steel. **Figure 3** indicates the each microchannel width of the Y-type microchannel. The water phase, the oil phase and the emulsion phase microchannel width are 141μm, 104μm and 137μm, respectively. The Y-type microchannel is 35 mm long, 60 mm wide and 21 mm thick.

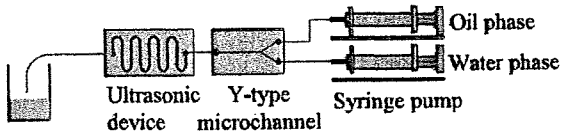

Fig. 1 Schema of the emulsion generating system

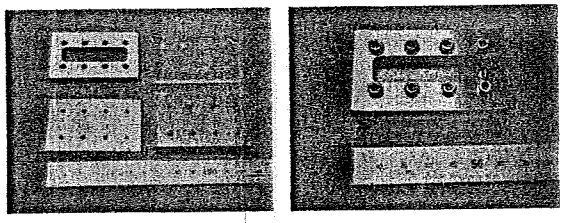

Fig. 2 Photographs of the Y-type microchannel

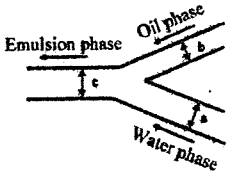

	Channel width (μm)
a	141
b	104
c	137

Fig. 3 Y-type microchannel's width

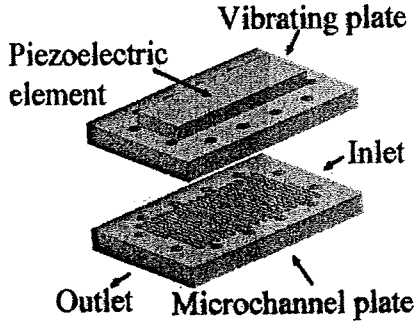

Fig. 4 Schematic view of ultrasonic device

The ultrasonic device consists of two plates. One is microchannel plate and the other is vibrating plate on which a piezoelectric element is bonded. The lead zirconate titanate (PZT) is used as piezoelectric element (Fuji Ceramics Co., Japan). These plates are made of stainless steel. These plates are clamped when they are used. **Figure 4** shows schematic view of the ultrasonic device.

The corss-sectional view and the top view of the microchannel are indicated in **Fig. 5**. The microchannel is 0.711mm wide and 0.35mm deep. Total length of the microchannel is 24 times of the top view in Fig. 4. The centerline of the microchannel is 1630.6mm and the volume of the microchannel is 342.4mm^3. The plate is 50mm long, 80mm wide and 5mm thick. The piezoelectric element is 20mm long, 60mm wide and 5mm thick. Photographs of the fabricated ultrasonic device are shown in **Fig. 6.**

2.2 Materials

Table I shows the materials used for generating emulsion in this study. The materials used were aqueous glycerol solution as water phase, tricaproin, tricaprylin, Tween 80 and egg yolk lecithin as oil phase 17). Tween 80 and egg yolk lecithin were used as a surfactant. These surfactants change the interfacial tension and make it easy to generate emulsions.

Table I Materials.

Water phase	Aqueous glycerol solution
Oil phase	Tricaproin,Tricaprylin, Tween 80,Egg yolk lecithin

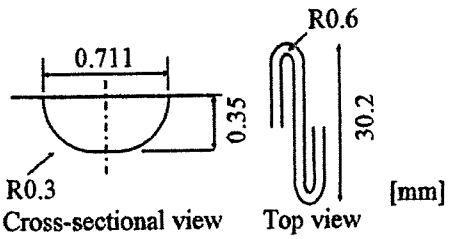

Fig. 5 Cross-sectional view (left) and top view (right) of the microchanne

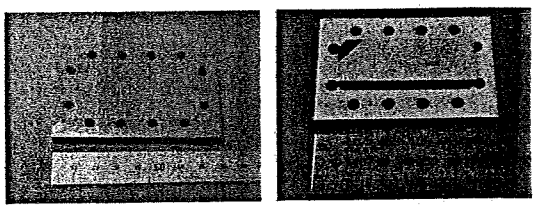

Fig. 6 Photographs of ultrasonic device: Microchannel plate (left) Vibrating plate (left)

3. Experimental results

3.1 FEM analysis

To confirm the vibrational mode and the resonance frequency of the vibrating plate, finite element method (FEM)

analysis was conducted by ANSYS. The analytical result is shown in **Fig .7**. As shown in Fig. 7, thickness vibration was generated and the resonance frequency was about 2.3MHz.

In addition, two-dimensional acoustic analysis was conducted to obtain the pressure distribution. The acoustic analytical result is shown in **Fig. 8**. Fig. 8 shows one of microchannle's acoustic analytical results of pressure distribution. The ultrasonic irradiation direction was from bottom to up in Fig. 8. From Fig. 8, pressure distribution was corresponding to the half length of the acoustic wave.

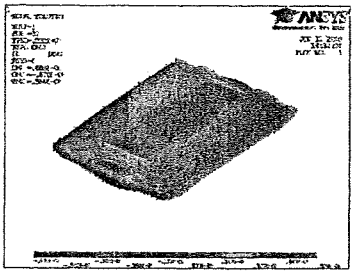

Fig .7 A vibrational mode of the vibrating plate by FEM: Frequency was about 2.3MHz

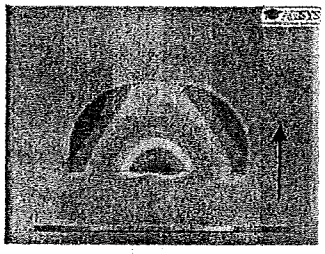

Fig .8 Pressure distribution in the microchannel in section by FEM

3.2 Evaluation of device performance

The relationship between the applied voltage and current was measured and the result is shown in **Fig. 9**. From the Fig. 9, the power consumption were 13.5, 31.2, 46.5W, when the applied voltage were $50V_{p\text{-}p}$, $80V_{p\text{-}p}$, $100V_{p\text{-}p}$, respectively.

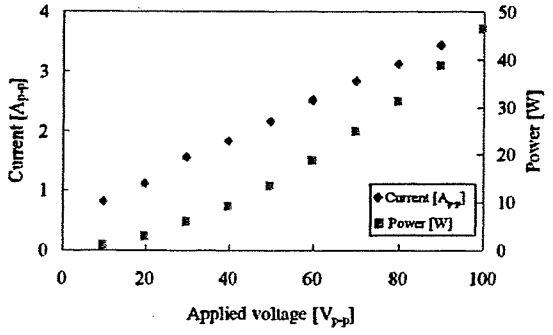

Fig. 9 Relationship between the applied voltage and electric current and power

The vibrational amplitude was measured by using a laser Doppler vibrometer. The vibrating plate was clamped at both ends when the vibrational amplitude was measured. **Figure 10** shows the schematic view of measurement area. The center of the plate was x origin and y origin and dots in Fig. 10 were measurement points. The vibrational amplitude was measured from the center to side to side at 5mm intervals to 20mm in x direction and up and down at 5mm intervals in y direction.

The relationship between the distance and the amplitude was shown in **Fig. 11**. From this result, vibration had slight variability on the sides of plate. This reason is considered that piezoelectric element and vibrating plate were not boned uniformly. Therefore, there was a slight variability on the sides of plate.

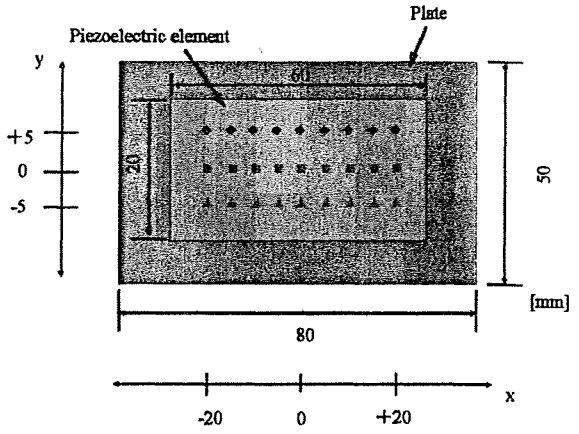

Fig. 10 Schematic view of measurement area

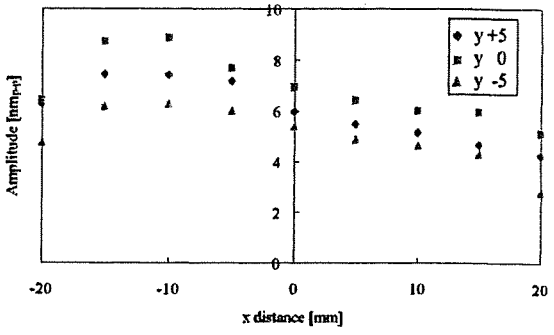

Fig. 11 Relationship between the distance and the amplitude

The temperature character of the ultrasonic device was measured. The experimental condition was that the applied voltage was $100V_{p\text{-}p}$ and driving frequency was 2.25MHz. The result was shown in **Fig. 12**. As shown in Fig. 12, the temperature was in thermal equilibrium in 15 minutes. The temperature was 90 degrees. This temperature increase caused by the ultrasonic device driving didn't effect generation of emulsion greatly.

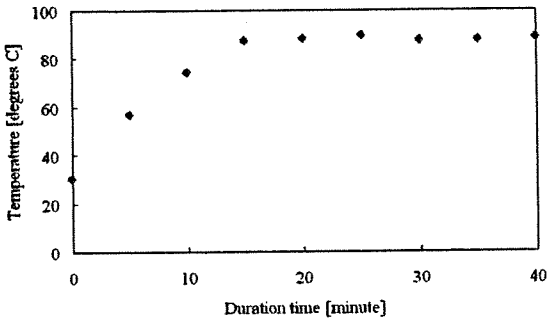

Fig. 12 Relationship between the duration time and the temperature

3.3 Emulsion generation

Firstly, the generation of emulsion by Y-type microchannel was conducted. The flow rate of the water phase and the oil phase were 100μl/min and 1μl/min, respectively. **Figure 13** shows the optical microscope photographs of generated emulsions by Y-type microchannel. According to Fig. 13, polydisperse emulsions were generated. Most diameters of the generated emulsions were about less than 50μm.

Table 2 shows the flow rate of the water phase and oil phase, applied voltage and driving frequency. The flow rate of the water phase and oil phase and driving frequency were constant value 100μl/min, 1μl/min, 2.25MHz, respectively. Applied voltage was changed $50V_{p\text{-}p}$, $80V_{p\text{-}p}$ and $100V_{p\text{-}p}$, respectively. **Figure 14** shows optical microscope photographs of the generated emulsions sonicated by ultrasonic device when applied voltages were $50V_{p\text{-}p}$, $80V_{p\text{-}p}$ and $100V_{p\text{-}p}$, respectively. From the comparison of Fig. 13 and Fig. 14, emulsions became so small that it is difficult to observe emulsions by optical microscope. **Figure 15** indicates the distribution of the emulsion diameter measured by the dynamic light scattering (DLS) when applied voltage were $50V_{p\text{-}p}$, $80V_{p\text{-}p}$, and $100V_{p\text{-}p}$, respectively. From Fig. 15, as the applied voltage increased, the peak wide around 200nm became sharper and the distribution around 6μm reduced. This result means that the ultrasonic irradiation intensity was important factor and as the ultrasonic irradiation intensity increased, generated emulsion became small and distribution became sharp. This result corresponded to the references.

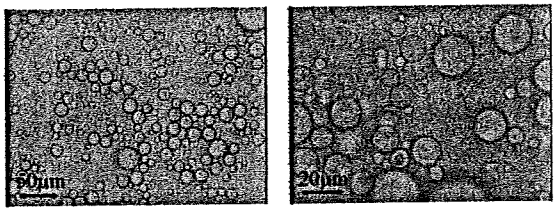

Fig. 13 Optical microscope photographs of generated emulsions by Y-type microchannel: The flow rate of the water phase and the oil phase were 100μl/min and 1μl/min.

Table 2 Flow rate, applied voltage and driving frequency.

	A	B	C
Water phase [μl/min]	100	100	100
Oil phase [μl/min]	1	1	1
Applied Voltage [$V_{p\text{-}p}$]	50	80	100
Power [W]	13.5	31.2	46.5
Driving frequency [MHz]		2.25	

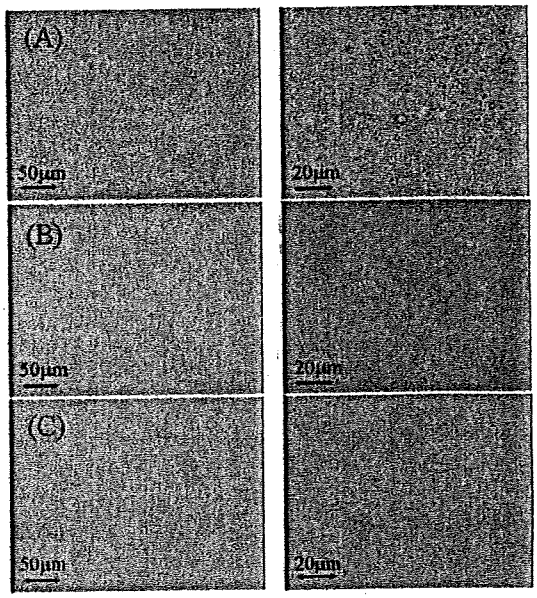

Fig. 14 Optical microscope photographs of generated emulsions by ultrasonic device: Upper (A) condition, middle (B) condition, under (C) condition

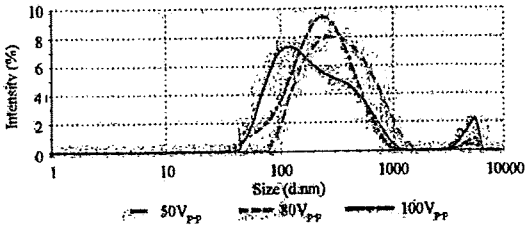

Fig. 15 Relationship between emulsion diameter and intensity measured by DLS when applied voltage was changed

Furthermore, the generation of emulsion by changing the flow rate of water and oil phase was conducted. This experiment's aim was to investigate the emulsion generation by the difference of the residence time. Table 3 shows the residence time, when the water and oil phase flow rates were 100-1μl/min, 200-2μl/min, and 50-0.5μl/min. The applied voltage and driving frequency were constant value $100V_{p\text{-}p}$ and 2.25MHz, respectively. Optical microscope photographs of